

Demonstration of a Time-Efficient Mobility System Using a Scaled Smart City

L. E. Beaver, B. Chalaki, A. M. Mahbub, L. Zhao, R. Zayas, A. A. Malikopoulos
University of Delaware, Department of Mechanical Engineering, Newark, DE, USA 19716

ARTICLE HISTORY

Compiled May 2, 2022

ABSTRACT

The implementation of connected and automated vehicle (CAV) technologies enables a novel computational framework to deliver real-time control actions that optimize travel time, energy, and safety. Hardware is an integral part of any practical implementation of CAVs, and as such, it should be incorporated in any validation method. However, high costs associated with full scale, field testing of CAVs have proven to be a significant barrier. In this paper, we present the implementation of a decentralized control framework, which was developed previously, in a scaled-city using robotic CAVs, and discuss the implications of CAVs on travel time. Supplemental information and videos can be found at <https://sites.google.com/view/ud-ids-lab/tfms?>.

KEYWORDS

Connected and automated vehicles; optimal control; emerging mobility systems; smart city; scaled city.

1. Introduction

Connectivity and automation provide the most intriguing opportunity for enabling users to better monitor transportation network conditions and make better operating decisions to reduce energy consumption, greenhouse gas emissions, travel delays, and improve safety (Fig. 1). The availability of vehicle-to-vehicle (V2V) and vehicle-to-infrastructure (V2I) communication has the potential to ease congestion and improve safety by enabling vehicles to respond rapidly to changes in their mutual environment. Furthermore, vehicle automation technologies can aim at developing vehicle control systems to account for unpredictable changes in local infrastructure.

With the advent of emerging information and communication technologies, we are witnessing a massive increase in the integration of our energy, transportation, and cyber networks, which, coupled with human factors, is giving rise to a new level of complexity in transportation networks [1]. As we move to increasingly complex emerging transportation systems, with changing landscapes enabled by connectivity and automation, future transportation networks could shift dramatically with the large-scale deployment of connected and automated vehicles (CAVs). On one hand, with the generation of massive amounts of data from vehicles and infrastructure, there are significant opportunities to develop optimization methods to identify and realize a sig-



Figure 1. A city enabled by connectivity and automation technologies.

nificant energy reduction of the transportation network, and to optimize the large-scale system behavior using the interplay between vehicles. On the other hand, evaluation and validation of new control approaches under different traffic scenarios is a necessity to ensure successful implementation per vehicle alongside desired system-level outcomes.

The overarching goal of this paper is the experimental demonstration of a decentralized control framework for CAVs presented in [2] using the University of Delaware’s Scaled Smart City (UDSSC). UDSSC is a 1:25 scaled test-bed representing an urban environment with robotic CAVs that can replicate real-world traffic scenarios in a controlled environment (Fig. 2). UDSSC can be used to explore the acquisition and processing of vehicle-to-vehicle and vehicle-to-infrastructure communication. It can also be used to validate control algorithms for coordination of CAVs in specific transportation scenarios, e.g., intersections, merging roadways, roundabouts, by mitigating the high costs and safety concerns associated with real-world field testing of CAVs.

The structure of the paper is organized as follows. In Section 2, we discuss related work on optimal control for CAVs reported in the literature. In Section 3, we review the decentralized control framework presented in [2] for coordination of CAVs in a transportation network. Then, we describe briefly the UDSSC test-bed in Section 4, and present simulation and experimental results in Section 5. Finally, we draw concluding remarks from the experiments in Section 6.

2. Related Work

CAVs have extensively been recognized [3,4] for the potential of improving mobility, safety, along with energy and emission reduction. There have been mainly two major approaches of utilizing connectivity and automation to improve transportation



Figure 2. The University of Delaware’s Scaled Smart City.

efficiency and safety.

The first approach utilizes connectivity and automation to form closely-coupled vehicular platoons to effectively reduce aerodynamic drag, especially at a high cruising speed. The concept of forming platoons of vehicles traveling at high speed was a popular system-level approach to address traffic congestion that gained momentum in the 1980s and 1990s [5,6]. An automated transportation system can alleviate congestion, reduce energy use and emissions, and improve safety while increasing throughput significantly. The Japan ITS Energy Project [7], the Safe Road Trains for the Environment program [8], and the California Partner for Advanced Transportation Technology [9], are among the mostly-reported efforts in this area.

The second approach is to smooth the traffic flow by *centralized* or *decentralized* vehicle control to reduce spatial and temporal speed variation and the events of braking, e.g., automated intersection crossing [10–12], cooperative merging [2,13,14], and speed harmonization through optimal vehicle control [15]. In centralized approaches, there is at least one task in the system that is globally decided for all vehicles by a single central controller, whereas in decentralized approaches, the vehicles are treated as autonomous agents that collect traffic information to optimize their specific performance criteria while satisfying physical constraints. One of the very early efforts in this direction was proposed by Athans [16] for safe and efficient coordination of merging maneuvers with the intention to avoid congestion. Since then, numerous approaches have been proposed on coordinating CAVs to improve traffic flow [17–19], and to achieve safe and efficient control of traffic through different traffic bottlenecks where potential vehicle collisions may happen [20–29]. In terms of energy impact, various studies have shown that significant fuel consumption savings could be achieved through eco-driving and vehicle optimal control without sacrificing driver safety [2,12–14,30–33]. Considering near-future CAV deployment, recent research work has also explored both traffic and energy implications of partial penetration of CAVs under different transportation scenarios, e.g., [34–36]. A survey of the research efforts in this area that have been reported in the literature to date can be found in [37–39].

Although previous work has shown promising results emphasizing the potential benefits of coordination of CAVs, validation has been primarily in simulation. In previous work, we presented the experimental validation of the solution of the unconstrained

merging roadway problem in UDSSC using 10 robotic CAVs [40]. In this paper, we demonstrate the impact of an optimal decentralized framework, developed in earlier work [2], for coordinating CAVs in a transportation network with multiple conflict zones where potential lateral collision may occur.

3. Decentralized Control Framework

We consider a network of CAVs driving in the roadway network in UDSSC that consists of several conflict zones, e.g., ramps, roundabouts, and intersections (as marked in red boxes in Fig. 3). The CAVs are retrofitted with the communication devices necessary to interact with other CAVs and structures within their communication range through V2V and V2I communication. Upstream of each conflict zone, we define a *control zone*, inside of which, CAVs can coordinate with each other to avoid any rear-end or lateral collisions in the conflict zone (Fig. 3). For each conflict zone, there is a coordinator that communicates with the CAVs traveling within the control range.

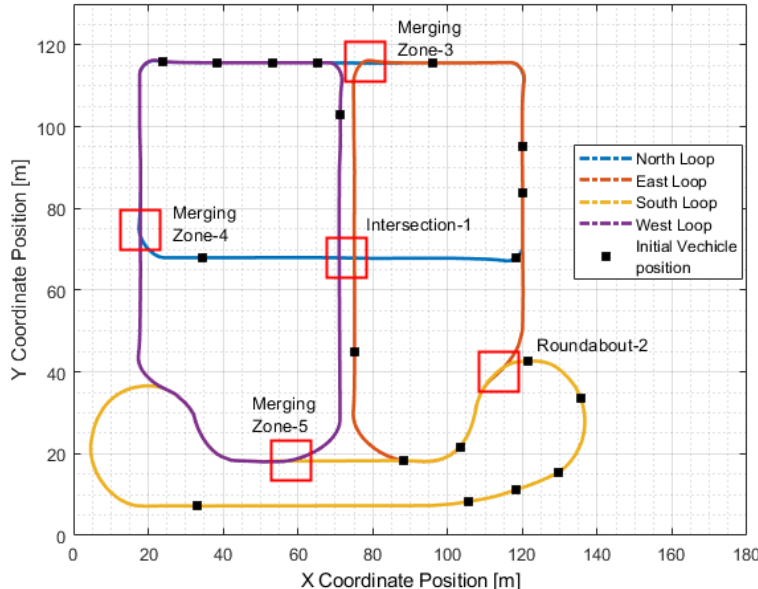


Figure 3. Vehicle routes in the University of Delaware's Scaled Smart City environment.

3.1. Modeling Framework and Assumptions

Let $z \in \mathcal{Z}$ be the index of a conflict zone in the corridor. Let $N(t) \in \mathbb{N}$ be a queue of CAVs to be analyzed at the time $t \in \mathbb{R}^+$. The dynamics of each vehicle $i, i \in \mathcal{N}(t)$, are represented with a state equation

$$\dot{x}(t) = f(t, x_i, u_i), \quad x_i(t_i^0) = x_i^0, \quad (1)$$

where $x_i(t), u_i(t)$ are the state of the vehicle and control input, t_i^0 is the initial time of vehicle i , and x_i^0 is the value of the initial state. For simplicity, we model each vehicle

as a double integrator, i.e., $\dot{p}_i = v_i(t)$ and $\dot{v}_i = u_i(t)$, where $p_i(t) \in \mathcal{P}_i$, $v_i(t) \in \mathcal{V}_i$, and $u_i(t) \in \mathcal{U}_i$ denote the position, speed, and acceleration/deceleration (control input) of each vehicle i . Let $x_i(t) = [p_i(t) \ v_i(t)]^T$ denotes the state of each vehicle i , with initial value $x_i^0(t) = [0 \ v_i^0(t)]^T$, taking values in the state space $\mathcal{X}_i = \mathcal{P}_i \times \mathcal{V}_i$. The sets \mathcal{P}_i , \mathcal{V}_i , and \mathcal{U}_i , $i \in \mathcal{N}(t)$, are complete and totally bounded subsets of \mathbb{R} . The state space \mathcal{X}_i for each vehicle i is closed with respect to the induced topology on $\mathcal{P}_i \times \mathcal{V}_i$ and thus, it is compact.

To ensure that the control input and vehicle speed are within a given admissible range, the following constraints are imposed:

$$\begin{aligned} u_{min} &\leq u_i(t) \leq u_{max}, \text{ and} \\ 0 &\leq v_{min} \leq v_i(t) \leq v_{max}, \forall t \in [t_i^0, t_i^f], \end{aligned} \tag{2}$$

where u_{min}, u_{max} are the minimum deceleration and maximum acceleration respectively, v_{min}, v_{max} are the minimum and maximum speed limits respectively, and t_i^0, t_i^f are the times that each vehicle i enters and exits the network.

To ensure the absence of rear-end collision of two consecutive vehicles traveling on the same lane, the position of the preceding vehicle should be greater than, or equal to the position of the following vehicle plus a predefined safe distance $\delta_i(t)$, where $\delta_i(t)$ is proportional to the speed of vehicle i , $v_i(t)$. Thus, we impose the rear-end safety constraint

$$s_i(t) = p_k(t) - p_i(t) \geq \delta_i(t), \quad \forall t \in [t_i^0, t_i^f], \tag{3}$$

where vehicle k is immediately ahead of i on the same lane.

Definition 1. Each CAV $i \in \mathcal{N}(t)$ belongs to at least one of the following two subsets of $\mathcal{N}(t)$ depending on its physical location inside the control zone: 1) $\mathcal{L}_i^z(t)$ contains all CAVs traveling on the same road and lane as vehicle i that may cause rear-end collision with vehicle i towards conflict zone z , and 2) $\mathcal{C}_i^z(t)$ contains all CAVs traveling on a different road from i and can cause lateral collision at the conflict zone z .

Definition 2. For each vehicle $i \in \mathcal{N}(t)$, we define the set Γ_i^z that includes only the positions along the lane where a lateral collision is possible in a conflict zone z , namely

$$\Gamma_i^z \triangleq \left\{ t \mid t \in [t_i^{z,m}, t_i^{z,f}] \right\}, \tag{4}$$

where $t_i^{z,m}$ is the time that vehicle i exits the control zone (and enters the conflict zone z), and $t_i^{z,f}$ is the time that vehicle i exits the conflict zone z .

Consequently, to avoid a lateral collision for any two vehicles $i, j \in \mathcal{N}(t)$ on different roads, the following constraint should hold

$$\Gamma_i^z \cap \Gamma_j^z = \emptyset, \quad j \in \mathcal{C}_i(t), \quad \forall t \in [t_i^{z,m}, t_i^{z,f}]. \tag{5}$$

The above constraint implies that only one vehicle at a time can be inside the conflict zone z . If the length of the conflict zone is long, then this constraint might not be realistic since it results in dissipating space and capacity of the road. However, the constraint is not restrictive in the problem formulation and it can be modified appropriately.

In the modeling framework described above, we impose the following assumptions:

Assumption 1. For each CAV i , none of the constraints is active at t_i^0 .

Assumption 2. Each CAV i has proximity sensors and can measure local information without errors or delays.

The first assumption ensures that the initial state and control input are feasible. The second assumption might be strong, but it is relatively straightforward to relax as long as the noise in the measurements and/or delays is bounded. For example, we can determine upper bounds on the state uncertainties as a result of sensing or communication errors and delays, and incorporate these into more conservative safety constraints.

3.2. Communication Structure

When a CAV $i \in \mathcal{N}(t)$ enters a control zone, it communicates with a coordinator, assigned to the corresponding conflict zone, and the other CAVs inside the control zone. Note that the coordinator is not involved in any decision for the CAVs and it only enables communication of appropriate information among vehicles. The coordinator handles the information between the vehicles as follows. When a vehicle enters the control zone at time t , the coordinator assigns a *unique identity* which is a pair (i, j) , where $i = N(t) + 1$ is an integer representing the location of the vehicle in a First-In-First-Out queue $\mathcal{N}(t)$ and $j \in \{1, 2\}$ is an integer based on a one-to-one mapping from $\mathcal{L}_i^z(t)$ and $\mathcal{C}_i^z(t)$ onto $\{1, 2\}$. If the vehicles enter the control zone at the same time, then the coordinator selects randomly their position in the queue.

Definition 3. For each CAV $i \in \mathcal{N}(t)$ entering the control zone z , the *information set* $Y_i^z(t)$, is defined as

$$Y_i^z(t) \triangleq \left\{ p_i(t), v_i(t), \mathcal{Q}^z, t_i^{z,0}, t_i^{z,m} \right\}, \forall t \in [t_i^{z,0}, t_i^{z,m}], \quad (6)$$

where $p_i(t), v_i(t)$ are the position and speed of CAV i inside the control zone z , $\mathcal{Q}^z \in \{\mathcal{L}_i^z(t), \mathcal{C}_i^z(t)\}$ is the subset assigned to CAV i by the coordinator, $t_i^{z,0}$ is the time when vehicle i enters the control zone for zone z , and $t_i^{z,m}$ is the time targeted for vehicle i to enter the conflict zone z . The set $Y_i^z(t)$ includes all information that each vehicle shares.

The time $t_i^{z,m}$ that the vehicle i will be entering the conflict zone z is restricted by the imposing rear-end and lateral collision constraints. Therefore, to ensure that (3) and (5) are satisfied at $t_i^{z,m}$ we impose the following conditions which depend on the subset that the vehicle $i - 1$ belongs to.

If $i - 1 \in \mathcal{L}_i^z(t)$,

$$t_i^{z,m} = \max \left\{ \min \left\{ t_{i-1}^{z,m} + \frac{\delta(t)}{v_z}, \frac{L^z}{v_{min}} \right\}, \frac{L^z}{v_i(t_i^{z,0})}, \frac{L^z}{v_{max}} \right\}. \quad (7)$$

If $i - 1 \in \mathcal{C}_i^z(t)$,

$$t_i^{z,m} = \max \left\{ \min \left\{ t_{i-1}^{z,m} + \frac{S^z}{v^z}, \frac{L^z}{v_{min}} \right\}, \frac{L^z}{v_i(t_i^{z,0})}, \frac{L^z}{v_{max}} \right\}, \quad (8)$$

where S^z is the length of conflict zone z , L^z is the length of control zone for zone z , v^z is the imposed speed inside the conflict zone z , and $v_i(t_i^{z,0})$ is the initial speed of vehicle i when it enters the control zone at $t_i^{z,0}$. The conditions (7) and (8) ensure that the time $t_i^{z,m}$ each vehicle i will be entering the conflict zone is feasible and can be attained based on the imposed speed limits inside the control zone. In addition, for low traffic flow where vehicle $i - 1$ and i might be located far away from each other, there is no compelling reason for vehicle i to accelerate within the control zone to have a distance $\delta(t)$ from vehicle $i - 1$, if $i - 1 \in \mathcal{L}_i^z(t)$, or a distance S^z if $i - 1 \in \mathcal{L}_i^z(t)$, at the time $t_i^{z,m}$ that vehicle i enters the conflict zone z . Therefore, in such cases vehicle i can keep cruising within the control zone with the initial speed $v_i(t_i^{z,0})$ that entered the control zone at $t_i^{z,0}$.

The recursion is initialized when the first vehicle enters the control zone z , i.e., it is assigned $i = 1$. In this case, $t_1^{z,m}$ can be externally assigned as the desired exit time of this vehicle whose behavior is unconstrained. Thus the time $t_1^{z,m}$ is fixed and available through $Y_1(t)$. The second vehicle will access $Y_1^z(t)$ to compute the times $t_2^{z,m}$. The third vehicle will access $Y_2^z(t)$ and the communication process will continue with the same fashion until the vehicle N in the queue access the $Y_{N(t)-1}^z(t)$.

3.3. Optimal Control Problem Formulation

We consider the problem of deriving the optimal control input (acceleration/deceleration) of each CAV inside each control zone separately under hard safety constraints to avoid collisions. By controlling the speed of the vehicles, the speed of queue built-up at each conflict zone decreases, and thus the congestion recovery time is also reduced. The latter results in maximizing the throughput in the merging zone. Moreover, by optimizing the acceleration/deceleration of each vehicle, we minimize transient operation, thus we can have direct benefits in energy since vehicles are optimized over steady state operating points (constant torque and speed).

Since the coordinator for a conflict zone z is not involved in any decision on the vehicle coordination, we formulate the following optimization problem for each vehicle in the queue towards conflict zone z that may be solved on line:

$$\min_{u_i} \frac{1}{2} \int_{t_i^{z,0}}^{t_i^{z,f}} u_i^2(t) dt, \quad \forall z \in \mathcal{Z}, \quad (9)$$

Subject to : (1), (2), $p_i(t_i^{z,0}) = p_i^{z,0}$, $v_i(t_i^{z,0}) = v_i^{z,0}$, $p_i(t_i^{z,f}) = p_z$,
and given $t_i^{z,0}$, $t_i^{z,f}$,

where p_z is the location (i.e., entry position) of conflict zone z , $p_i^{z,0}$, $v_i^{z,0}$ are the initial position and speed of vehicle i when it enters the control zone of conflict zone z .

For the analytical solution and real-time implementation of the control problem (9), we apply Hamiltonian analysis. In our analysis, we consider that when the vehicles enter the control zone, none of the state and control constraints in (2) are active.

The analytical solution of (9) without considering state and control constraints was presented in earlier papers [13,14] for coordinating CAVs in real time at highway on-ramps and [33] at two adjacent intersections. When the state and control constraints are not active, the optimal control input (acceleration/deceleration) as a function of time is given by

$$u_i^*(t) = a_i t + b_i, \quad (10)$$

and the optimal speed and position for each vehicle are

$$v_i^*(t) = \frac{1}{2} a_i t^2 + b_i t + c_i, \quad (11)$$

$$p_i^*(t) = \frac{1}{6} a_i t^3 + \frac{1}{2} b_i t^2 + c_i t + d_i, \quad (12)$$

where a_i, b_i, c_i and d_i are constants of integration. These constants can be computed by using the initial and final conditions. Since we seek to derive the optimal control (10) in real time, we can designate initial values $p_i(t_i^{z,0})$ and $v_i(t_i^{z,0})$, and initial time, $t_i^{z,0}$, to be the current values of the states $p_i(t)$ and $v_i(t)$ and time t , where $t_i^{z,0} \leq t \leq t_i^{z,m}$.

Similar results to (10)-(11) can be obtained when the state and control constraints become active within the control zone. To address the problem of the constraint violations in (2), the constrained and unconstrained arcs need to be pieced together to satisfy the Euler-Lagrange equations and necessary condition of optimality. Although we have two state constraints and two control constraints from (2), the nature of the unconstrained optimal control dictates that it is only possible for a subset of the constraints to be active within an unconstrained solution. For example, if one of the state constraint $v_i(t) - v_{max} < 0$ is violated in the unconstrained arc, the other state constraint $v_{min} - v_i(t) < 0$ cannot be violated within the control zone. Therefore, it is not necessary to consider all the cases while solving for the constrained case, which reduces computational redundancy. The different cases of the state and control constraint activation and the corresponding solution can be found in [12]. In the present work, we do not consider any constrained optimization cases as none of the constraints in (2) become active within the optimal control path during the simulation. We validate this claim with the simulation result presented in section 5.

4. Simulation and Experimental Environment

4.1. Simulation Setup

To implement the control framework presented in the previous section and to generate the input information required for UDSSC, we first use the microscopic multi-modal simulation platform PTV VISSIM. We create a simulation setup replicating the UDSSC map and define a network consisting of four different looped routes and five sources of bottleneck (one intersection, one roundabout, and three merging scenario), as shown in Fig. 3. In order to maintain compatibility with the UDSSC experiment, we design each of the routes to hold finite number of vehicles (19 vehicles in total) travelling in loops for finite simulation run-time. Among the 19 vehicles, we consider 9 vehicles as the target (ego-vehicles) to evaluate their performance metrics in different

scenarios. We use the rest of the vehicles to increase the traffic volume in the urban network and create congestion in the baseline scenario. The vehicles maintain a low desired speed of 7 m/s for their uncontrolled urban commute throughout the network. Therefore, the desired speed at all exits of the control zones is set to be equal to the urban speed. We select the maximum and minimum allowable speed of 8.33 m/s and 2 m/s respectively. The maximum and minimum acceleration of the vehicles have been considered as 3 m/s^2 and -3 m/s^2 respectively. To evaluate the effectiveness of the proposed optimal vehicle dynamics control, we consider two different cases:

a. Baseline Scenario: We construct the baseline scenario considering all the vehicles to be human driven and without any vehicle-to-vehicle (V2V) communication capability. The vehicles subscribe to the VISSIM built-in Wiedemann car following model to emulate the driving behavior of real human driven vehicles. We build a fixed time signalized intersection for the four-way traffic at the center and adopt priority based (yield/stop) movement for the other four waypoints consisting of the roundabout and merging scenarios.

b. Optimal Controlled Scenario: In the optimal scenario, all the vehicles are connected with each other inside the control zone through V2V communication capability and are automated within the control zone. Therefore, they can plan their optimal path inside the control zone avoiding any lateral or rear-end collision and optimize their individual travel time and fuel efficiency. In this scenario, we do not consider the fixed-time signal and movement priorities considered in the baseline case. We consider five isolated coordinators with a control zone of 45 m for each conflict zone (see Fig. 3). For the uncontrolled paths in-between the control zones, the vehicles adopt the Wiedemann car following model [41] to traverse their respective routes.

4.2. University of Delaware's Scaled Smart City

The UDSSC is a 1:25 scaled test-bed spanning over 400 square feet (see Fig. 2) and is capable of accommodating at least 25 scaled CAVs. It is equipped with a VICON motion capture system which uses eight cameras to track the position of each vehicle with sub-millimeter accuracy. Each road in the UDSSC is built up from arc or line segments. In order to track the desired vector position of each CAV, all road segments are parameterized in terms of their total length. This formulation allows each vehicle to calculate its desired position in UDSSC based only on the scalar distance along its current path, which is achieved by numerically integrating the speed profile in real-time on both the mainframe computer and the CAV. This decoupling of speed and position allows significant flexibility in UDSSC, especially in dynamic-routing scenarios.

4.2.1. Connected and Automated Vehicles

The CAVs of UDSSC (see Fig. 4) have been designed using off the shelf electrical components and 3D printed parts created at the University of Delaware. The primary microcontroller on the CAV is a Raspberry Pi 3B running Ubuntu Mate and ROS Kinetic. An Arduino Nano is used as a slave processor for Pi to do a low-level motor control and ad-hoc analog to digital conversion for SOC measurements. The CAV's rear-wheel drive train is powered by a pololu 75.8:1, 6 V micro metal gearmotor; the motor is controlled using a motor controller, and encoder for feedback, hooked into the Arduino. Power from the gearmotor is transferred to the rear axle with two 3D printed gears with a 1:1 ratio, and two rubberized wheels with radius $r = 1.6 \text{ cm}$ are mounted directly to the rear axle. The motor controller receives power through a



Figure 4. A picture of the connected and automated vehicle’s electronics (left) and outer shell with VICON markers, ultrasonic sensors, and camera visible (right).

5 V regulator, and a pulse-width modulated command from the Arduino is used to control the motor’s speed. Steering is achieved by a custom 3D printed ackermann-style steering mechanism actuated by a Miuzei micro servo motor, which again is controlled directly by the Arduino. The CAVs are also equipped with a Pi Camera, ultrasonic sensors, and a SOC measurement circuit to collect experimental data and reduce the overall reliance on VICON. A power regulator manages the voltage requirement of the Pi and Arduino by supplying a regulated 5 V DC from two 3000 mAh 3.7 V Li-ion batteries configured in series. With this hardware configuration, the CAV is able to run and collect experimental data at 20 Hz for up to 2 hours.

4.2.2. Control System Architecture

Coordination of the CAVs within the UDSSC is achieved using a multi-level control framework spanning a central *mainframe* computer (Processor: Intel Core i7-6950X CPU @ 3.00 GHz x 20, Memory: 125.8 Gb) and the individual CAVs in the experiment (Raspberry Pi 3B). The mainframe runs an Ubuntu 16.04.5 LTS Linux distribution and ROS Kinetic. High level routing is achieved by a multithreaded C++ program running on the mainframe computer. For this set of experiments the mainframe is initialized with the path information and speed profiles for each CAV. At the start of the experiment each CAV sets its temporal baseline from which it measures all later times; this avoids the problem of synchronizing CAV clocks, as all information is calculated relative to the experiment start. During the experiment the mainframe passes a message to each CAV containing its current position and two seconds of trajectory data using the UDP/IP protocol at 50 Hz. The CAV receives trajectory information from the mainframe and uses a modified Stanley [42] and feedforward-feedback [43] controller to handle lane and speed tracking.

Medium and low-level control is accomplished on board each CAV in a purely distributed manner. Using information from the mainframe, each vehicle’s Raspberry Pi updates at 50 Hz to calculate a lateral, heading, and distance error. The lateral and heading errors are then passed to the Stanley controller to calculate an output steering angle. Meanwhile, the position error and desired speed are used in a feedforward-feedback controller to calculate a desired motor speed. The desired speed and steering

angle are then passed to the Arduino Nano which runs a low-level PID controller to precisely control the gearmotor and steering servo.

4.3. Experimental Setup

To replicate the simulation results in the UDSSC, speed profiles from VISSIM are exported into the mainframe. The path information and speed profile are dispersed to each CAV over the duration of the experiment. Then, the CAVs at UDSSC begin to numerically integrate the speed profile data in real time to calculate a desired position, allowing them to track the desired speed and position in a decentralized approach. Simultaneously, the mainframe computer integrates the speed profile in order to send the path information to the CAVs.

5. Results

5.1. Simulation Results

The speed and acceleration profiles of the CAVs making multiple passes through the north loop of the UDSSC map for the baseline and optimal control scenario are shown in Fig. 5a and Fig. 5b respectively. The north loop contains 4 vehicles traversing sequentially intersection-1, merging zone-4 and merging zone-3 in loop. From the speed profiles illustrated in Fig. 5a, we can see stop-and-go driving behavior in these cases. In the acceleration profile shown in Fig. 5a, we see extreme deceleration event in some cases which can have an impact on passenger discomfort. Note that, the effect of congestion in these cases can induce artificial congestion or *phantom traffic jam* outside the corridor, as it can be seen in Fig. 5a near the 50 m region.

The speed and acceleration profiles of the CAVs travelling through the same route under the optimal control framework is shown in Fig. 5b. Compared to the baseline speed profiles in Fig. 5a, we note that the speed profiles of the optimal control in Fig. 5b have completely eliminated stop-and-go driving showing an optimal quadratic profile within the control zones. The congestion observed in the baseline scenario in Fig. 5a has also been mitigated, rendering an overall smooth traffic flow throughout the network. Additionally, the acceleration of the CAVs in Fig. 5b have optimal linear profile which minimizes the transient motor operation.

Note that, the speed and acceleration profiles are kept within the maximum and minimum limit inside the control zone (Fig. 5b) as described in Section 4.1. Therefore, none of the state and control constraints of (2) became active in the unconstrained arc and our relaxation of (2) holds. However, we see a few cases of constraint violation of the acceleration profile outside the control zone in Fig. 5a, where the Wiedemann car-following model is applied instead of the optimal control. Note the optima control is applied only inside the designated control zones.

5.2. Experimental Validation

To validate the effectiveness of the efficiency of the optimal control observed in the simulation, we compare the travel time of 9 CAVs between the baseline and optimal scenarios. The travel time is calculated as the time taken for each vehicle to complete a single loop by sampling the raw VICON data over the 80 sec experiment. In particular, returning to the initial position was defined as the first time the vehicle came within

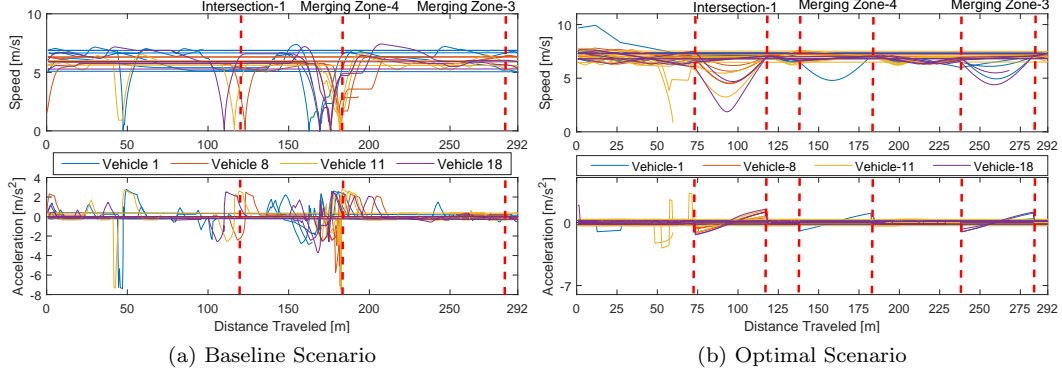


Figure 5. Speed and acceleration profiles of vehicles in the north loop under the baseline and optimal control scenarios.

10 cm of its initial position after a 5 sec initial window. These values are presented in Table 1 and Fig. 6 alongside the route each CAV took (as annotated in Fig. 3); a value of greater than 80 sec corresponds to a vehicle not fully completing its loop during the experiment, which occurred 3 times in the baseline scenario. Videos of the experiment can be found at the supplemental site, <https://sites.google.com/view/ud-ids-lab/tfms?>.

Table 1. Travel time for each vehicle to complete a single loop.

Vehicle	Baseline time [sec]	Optimal time [sec]	Loop	Time saved [sec]
8	> 80	54.10	North	> 25.9
18	> 80	48.00	North	> 32.0
12	66.25	45.55	East	20.70
14	65.95	49.90	East	16.05
4	57.80	53.25	South	4.55
13	60.30	59.75	South	0.55
2	46.61	37.40	West	9.21
5	43.90	44.20	West	-0.30
17	> 80	41.50	West	> 38.5

From Table 1 an average improvement of at least 16.35 sec (25%) of the baseline travel time, was observed in the UDSSC. The least significant improvement was in the Southern loop, where the traffic was effectively free-flowing in the baseline scenario. In the loops with conflict zones, i.e., north, east, and west, the impact of the coordinator and optimal control is clear and significant.

The speed profiles of some CAVs, e.g., 2, 14, 17, and 13, are shown in Fig. 7. These profiles were taken by numerically deriving the VICON position data taken at 100Hz to get velocity components. Then, any speeds above 0.8 m/s, well above the maximum speed of the CAVs, was attributed to occlusion during the experiment and discarded. Finally, the velocity magnitude was run through a moving average filter with a window of 0.45 sec.

From the results shown in Fig. 7 we can conclude that: 1) almost the entire reduction in transit time can be attributed to optimal control in the conflict zones and 2) the optimal control framework almost entirely eliminates stop-and-go driving.

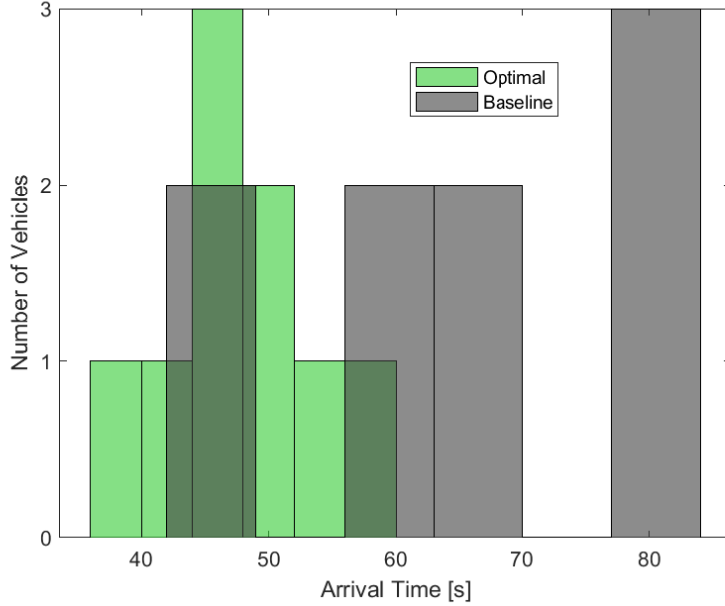


Figure 6. Histogram for the arrival time of each vehicle in Table 1 with 6 bins per experiment.

6. Conclusion

We presented an experimental demonstration of a decentralized optimal control framework for CAVs, presented in [2], using a 1:25 scaled test-bed representing an urban environment with robotic CAVs that can replicate real-world traffic scenarios in a controlled environment. We show that the optimal control framework can contribute a 25% reduction in travel time compared to a baseline scenario consisting of human-driven vehicles without connectivity.

Ongoing research is considering lane changing and exploring the associated tradeoffs between throughput and energy consumption of each individual vehicle. An important direction for future research is to consider different penetrations of CAVs, which can alter significantly the efficiency of the entire system. For example, an important question that need to be addressed is “what is the minimum number of CAVs in order to realize potential benefits?”

Acknowledgement(s)

The authors would like to acknowledge Michael Lashner, Kunzheng Li, Haley Lloyd, Thomas Patterson, and the rest of the the UDSSC Senior Design team for their effort in designing, building, and testing the newest generation of CAVs used in this paper. The authors would also like to thank Ioannis Vasileios Chremos for his valuable comments and feedback on the manuscript.

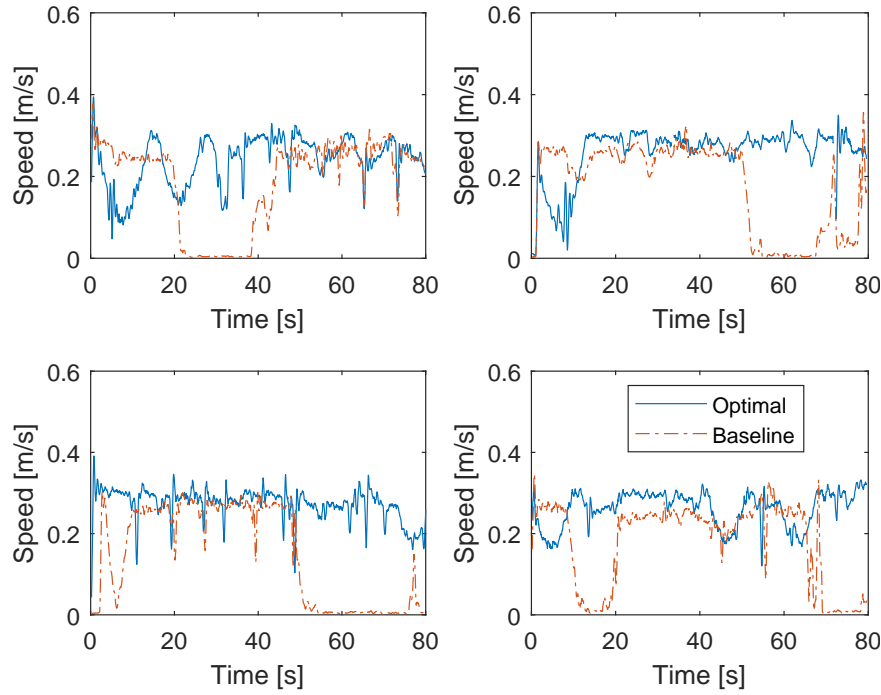


Figure 7. Speed vs time profiles for vehicles (clockwise from top left) 2 (west), 14 (east), 17 (west), 13 (south.).

Funding

This research was supported by the Delaware Energy Institute (DEI). This support is gratefully acknowledged.

References

- [1] Malikopoulos AA. A duality framework for stochastic optimal control of complex systems. *IEEE Transactions on Automatic Control*. 2016;61(10):2756–2765.
- [2] Zhao L, Malikopoulos AA. Decentralized optimal control of connected and automated vehicles in a corridor. In: 2018 21st International Conference on Intelligent Transportation Systems (ITSC); IEEE; 2018. p. 1252–1257.
- [3] Spieser K, Treleaven K, Zhang R, et al. Toward a systematic approach to the design and evaluation of automated mobility-on-demand systems: A case study in singapore. In: *Road vehicle automation*. Springer; 2014. p. 229–245.
- [4] Fagnant DJ, Kockelman KM. The travel and environmental implications of shared autonomous vehicles, using agent-based model scenarios. *Transportation Research Part C: Emerging Technologies*. 2014;40:1–13.
- [5] Shladover SE, Desoer CA, Hedrick JK, et al. Automated vehicle control developments in the PATH program. *IEEE Transactions on Vehicular Technology*. 1991;40(1):114–130.
- [6] Rajamani R, Tan HS, Law BK, et al. Demonstration of integrated longitudinal and lateral control for the operation of automated vehicles in platoons. *IEEE Transactions on Control Systems Technology*. 2000;8(4):695–708.
- [7] Tsugawa S. An overview on an automated truck platoon within the energy its project. *IFAC Proceedings Volumes*. 2013;46(21):41–46.
- [8] Dávila A, Nombela M. Sartre: Safe road trains for the environment. In: *Conference on*

Personal Rapid Transit PRT@ LHR; Vol. 3; 2010. p. 2–3.

[9] Shladover SE. Path at 20 history and major milestones. *IEEE Transactions on intelligent transportation systems*. 2007;8(4):584–592.

[10] Lee J, Park B. Development and Evaluation of a Cooperative Vehicle Intersection Control Algorithm Under the Connected Vehicles Environment. *IEEE Transactions on Intelligent Transportation Systems*. 2012;13(1):81–90.

[11] Rakha H, Kamalanathsharma RK. Eco-driving at signalized intersections using v2i communication. In: Intelligent Transportation Systems (ITSC), 2011 14th International IEEE Conference on; IEEE; 2011. p. 341–346.

[12] Malikopoulos AA, Cassandras CG, Zhang YJ. A decentralized energy-optimal control framework for connected automated vehicles at signal-free intersections. *Automatica*. 2018;93:244 – 256.

[13] Rios-Torres J, Malikopoulos AA. Automated and Cooperative Vehicle Merging at Highway On-Ramps. *IEEE Transactions on Intelligent Transportation Systems*. 2017;18(4):780–789.

[14] Ntousakis IA, Nikолос IK, Papageorgiou M. Optimal vehicle trajectory planning in the context of cooperative merging on highways. *Transportation Research Part C: Emerging Technologies*. 2016;71:464–488.

[15] Malikopoulos AA, Hong S, Park B, et al. Optimal control for speed harmonization of automated vehicles. *IEEE Transactions on Intelligent Transportation Systems*. 2018;.

[16] Athans M. A unified approach to the vehicle-merging problem. *Transportation Research*. 1969;3(1):123–133.

[17] Kachroo P, Li Z. Vehicle merging control design for an automated highway system. In: Proceedings of Conference on Intelligent Transportation Systems; 1997. p. 224–229.

[18] Antoniotti M, Deshpande A, Girault A. Microsimulation analysis of automated vehicles on multiple merge junction highways. *IEEE International Conference in Systems, Man, and Cybernetics*. 1997;:839–844.

[19] Ran B, Leight S, Chang B. A microscopic simulation model for merging control on a dedicated-lane automated highway system. *Transportation Research Part C: Emerging Technologies*. 1999;7(6):369–388.

[20] Dresner K, Stone P. Multiagent traffic management: a reservation-based intersection control mechanism. In: Proceedings of the Third International Joint Conference on Autonomous Agents and Multiagents Systems; 2004. p. 530–537.

[21] Dresner K, Stone P. A multiagent approach to autonomous intersection management. *Journal of artificial intelligence research*. 2008;31:591–656.

[22] de La Fortelle A. Analysis of reservation algorithms for cooperative planning at intersections. 13th International IEEE Conference on Intelligent Transportation Systems. 2010 Sep;:445–449.

[23] Huang S, Sadek A, Zhao Y. Assessing the Mobility and Environmental Benefits of Reservation-Based Intelligent Intersections Using an Integrated Simulator. *IEEE Transactions on Intelligent Transportation Systems*. 2012;13(3):1201–1214.

[24] Zohdy IH, Kamalanathsharma RK, Rakha H. Intersection management for autonomous vehicles using iCACC. 2012 15th International IEEE Conference on Intelligent Transportation Systems. 2012;:1109–1114.

[25] Yan F, Dridi M, El Moudni A. Autonomous vehicle sequencing algorithm at isolated intersections. 2009 12th International IEEE Conference on Intelligent Transportation Systems. 2009;:1–6.

[26] Li L, Wang FY. Cooperative Driving at Blind Crossings Using Intervehicle Communication. *IEEE Transactions in Vehicular Technology*. 2006;55(6):1712,1724.

[27] Zhu F, Ukkusuri SV. A linear programming formulation for autonomous intersection control within a dynamic traffic assignment and connected vehicle environment. *Transportation Research Part C: Emerging Technologies*. 2015;.

[28] Wu J, Perronnet F, Abbas-Turki A. Cooperative vehicle-actuator system: a sequence-based framework of cooperative intersections management. *Intelligent Transport Systems*,

IET. 2014;8(4):352–360.

[29] Kim KD, Kumar P. An MPC-Based Approach to Provable System-Wide Safety and Liveness of Autonomous Ground Traffic. *IEEE Transactions on Automatic Control*. 2014; 59(12):3341–3356.

[30] Barth M, Boriboonsomsin K. Energy and emissions impacts of a freeway-based dynamic eco-driving system. *Transportation Research Part D: Transport and Environment*. 2009; 14(6):400–410.

[31] Berry IM. The effects of driving style and vehicle performance on the real-world fuel consumption of us light-duty vehicles [dissertation]. Massachusetts Institute of Technology; 2010.

[32] Wu C, Zhao G, Ou B. A fuel economy optimization system with applications in vehicles with human drivers and autonomous vehicles. *Transportation Research Part D: Transport and Environment*. 2011;16(7):515–524.

[33] Zhang Y, Malikopoulos AA, Cassandras CG. Optimal control and coordination of connected and automated vehicles at urban traffic intersections. In: *Proceedings of the American Control Conference*; 2016. p. 6227–6232.

[34] Zhao L, Malikopoulos AA, Rios-Torres J. Optimal control of connected and automated vehicles at roundabouts: An investigation in a mixed-traffic environment. In: *15th IFAC Symposium on Control in Transportation Systems*; 2018. p. 73–78.

[35] Rios-Torres J, Malikopoulos AA. Impact of partial penetrations of connected and automated vehicles on fuel consumption and traffic flow. *IEEE Transactions on Intelligent Vehicles*. 2018;3(4):453–462.

[36] Zhong Z, Joyoung L, Zhao L. Evaluations of Managed Lane Strategies for Arterial Deployment of Cooperative Adaptive Cruise Control . In: *TRB Annual Meeting*; Washington DC, USA; 2017.

[37] Rios-Torres J, Malikopoulos AA. A Survey on Coordination of Connected and Automated Vehicles at Intersections and Merging at Highway On-Ramps. *IEEE Transactions on Intelligent Transportation Systems*. 2017;18(5):1066–1077.

[38] Guanetti J, Kim Y, Borrelli F. Control of connected and automated vehicles: State of the art and future challenges. *Annual Reviews in Control*. 2018;.

[39] Wang Y, Li X, Yao H. Review of trajectory optimisation for connected automated vehicles. *IET Intelligent Transport Systems*. 2018;.

[40] Stager A, Bhan L, Malikopoulos A, et al. A Scaled Smart City for Experimental Validation of Connected and Automated Vehicles. *IFAC-PapersOnLine*. 2018;51(9):130–135.

[41] Wiedemann R. *Simulation des strassenverkehrsflusses* [dissertation]. Universitat Karlsruhe; 1974.

[42] Thrun S, Montemerlo M, Dahlkamp H, et al. *Stanley: The robot that won the DARPA Grand Challenge*. Springer Tracts in Advanced Robotics. 2007;.

[43] Spong MW, Hutchinson S, Vidyasagar M. *Robot Dynamics and Control* Second Edition; 2004.